High-energy proton generation and suppression of transverse proton divergence by localized electrons in a laser-foil interaction

S. Miyazaki,[1,*] S. Kawata,[2,†] R. Sonobe,[2] and T. Kikuchi[2]
[1]*Department of Material Science and Engineering, Utsunomiya University, Yohtoh 7-1-2, Utsunomiya 321-8585, Japan*
[2]*Department of Electrical and Electronic Engineering, Utsunomiya University, Yohtoh 7-1-2, Utsunomiya 321-8585, Japan*
(Received 2 December 2004; published 9 May 2005)

A suppression of a transverse divergence of high-energy protons generated by an interaction of a laser with a thin slab foil is investigated in this paper by 2.5-dimensional particle-in-cell simulations. When an intense ($\sim 10^{24}$ W/m^2) short-pulse (a few ten femtoseconds) laser illuminates a thin foil target of a hydrogen, foil electrons are accelerated and compressed longitudinally by a laser light pressure and fast electron bunches are produced in the thin foil target. The fast electron bunches pass through the foil target, and a strong magnetic field is produced near the opposite side of the foil target. Because the strong magnetic field confines the electrons, a localization of the electrons is observed at the opposite side of a laser illumination surface. The local electron bunch produces not only a longitudinal electric field, but also a transverse electric field, which is directed toward the laser axis. Protons are accelerated and extracted from the foil, and the proton bunch divergence is successfully suppressed by the transverse electric field.

DOI: 10.1103/PhysRevE.71.056403 PACS number(s): 52.38.Kd, 52.65.Rr, 41.75.Jv

I. INTRODUCTION

With the development of a laser technology, a laser intensity of $I > 10^{24}$ W/m^2 has been achieved in recent years [1,2]. Intense lasers provide a strong electric field gradient of a few TV/m, and various interesting researches have been explored in a laser-matter interactions, such as direct electron acceleration in vacuum [3–9], high-energy ion sources [10–23], and so on. In this paper, we focus on high-energy proton production in a laser-foil interaction.

When an intense laser illuminates a thin slab foil, foil electrons obtain a net energy by the ponderomotive force of the laser and oscillate around the thin foil target, and the electrons cause a charge separation [10]. Foil ions are accelerated by an electric field generated by the charge separation and are emitted from both the sides of the foil target. On the side irradiated by the laser, the charge separation is mainly caused by hot electrons. On another side, the electrons accelerated by the ponderomotive force pass through the foil target and produce the charge separation. In recent theoretical and experimental results, ions energies of a few MeV or more have already been observed. In the future, an improvement in a quality of the ions accelerated becomes very important for applications to technology, and research in the progress of the ion beam qualities has just started [11,12]. In this paper, we perform 2.5-dimensional particle-in-cell (PIC) simulations to investigate the transverse proton beam divergence. We demonstrate that even in the slab target, a transverse proton divergence can be suppressed by the localization of an electron cloud in transverse.

In the laser-foil interactions, the behavior of electrons influences directly the ion dynamics. A part of the electrons placed at the surface irradiated by the laser is accelerated by the ponderomotive force and passes through the foil target. At the same time, a high current flows in the foil target and a magnetic field is also generated. Recently Ref. [11] proposed to employ an underdense plasma foil for effective proton acceleration. The intense laser propagates in the underdense plasma and accelerates the plasma electrons. The electrons accelerated produce a strong magnetic field, which has an electron confinement effect, and generate an electric field for a long time. Consequently the proton energy is higher than that in the case of an overdense plasma in the same parameter ranges [11].

In our study, we employ an intense short-pulse laser and a hydrogen foil target to suppress the transverse divergence of high-energy protons. In the case of an ultraintense and short-pulse laser, the electrons are accelerated and compressed longitudinally by the longitudinal ponderomotive force and produce fast electron bunches in the foil target. The fast electron bunches create the strong magnetic field and are confined by the magnetic field in the transverse direction. Therefore the fast electrons are localized in transverse and longitudinal directions at the target surface and the charge separation appears locally. Then the protons are mainly accelerated in the longitudinal direction and at the same time experience a transverse electric field generated by the electrons. Therefore the proton divergence can be suppressed. Consequently even in the slab target one can expect the suppression effect on the high-energy proton transverse divergence. In our suppression mechanism, the structure of the fast electrons influences the transverse proton divergence. In this paper, in order to investigate the localization effect of electrons, we calculate six different cases for the laser intensity and pulse duration for a fixed laser input energy. Our calculation results indicate that the maximum proton kinetic energy and average proton kinetic energy reach about 8 MeV and 3 MeV, respectively for all cases. In the case of higher intensity, the electrons are accelerated sufficiently, the magnetic field becomes strong, and the electrons are well localized. Therefore the transverse

*Corresponding authors. Electronic address: dt030106@cc.utsunomiya-u.ac.jp
†Corresponding authors. Electronic address: kwt@cc.utsunomiya-u.ac.jp

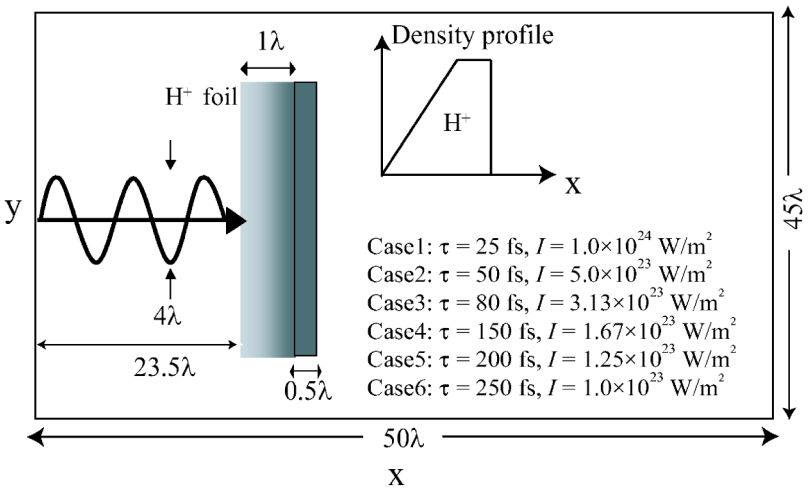

FIG. 1. Schematic view of the 2.5-dimensional particle-in-cell (PIC) simulations. The laser propagates in the x direction and is polarized in the y direction. The foil target consisting of hydrogen with a solid density. The thickness of the foil target is $\delta_f=1.5\lambda$ with an additional linearly changing density gradient of 1.0λ, where $\lambda=1.053\ \mu$m is the laser wavelength. The laser diameter $r_{spot}=4.0\lambda$. We perform the six different combinations of the laser intensity I and pulse duration τ, and the laser input energy is kept constant. The calculation region is given by $R=\{(x,y)|0<x<50\lambda, 0<y<45\lambda\}$, and the foil is placed in $23.5\lambda\leqslant x\leqslant 25\lambda$, and $10\lambda\leqslant y\leqslant 35\lambda$ at the initial time of $t=0$.

proton divergence becomes small compared those in the cases with the low laser intensities.

II. SIMULATION MODEL

In this section, we present the simulation model of 2.5-dimensional PIC simulations and the parameter set employed. Figure 1 shows a schematic view of our simulation model. It was found that an energy absorption coefficient from the laser to the target rises by preparing a density gradient at the laser illumination surface of the target [13]. In our calculation model, a hydrogen foil target with an additional linearly changing density gradient is employed. In this paper, the foil thickness $\delta_f=1.5\lambda$ and the width of the density gradient $\delta_{grad}=1.0\lambda$, where $\lambda=1.053\ \mu$m is the laser wavelength. The peak density of the target is its solid density ($n_e=n_i=42n_c$). Here n_e and n_i are the electron and proton number densities, respectively, and n_c is the critical density. Initially, the electrons and protons are in a Maxwell distribution with 1.0 keV. The mass ratio of the proton and electron is $m_i/m_e=1836$. The laser propagates in the x direction and is linearly polarized in the y direction with the Gaussian profile in the transverse and longitudinal directions. At the initial time, the laser enters at the left boundary and propagates in the x direction. The laser diameter $r_{spot}=4.0\lambda$. In order to investigate the magnetic field effect on the electrons, we perform six different cases of laser intensity I and pulse duration τ with the same fixed laser energy: $I=1\times10^{24}$ W/m^2 and $\tau=25$ fs (case 1), $I=5\times10^{23}$ W/m^2 and $\tau=50$ fs (case 2), $I=3.13\times10^{23}$ W/m^2 and $\tau=80$ fs (case 3), $I=1.67\times10^{23}$ W/m^2 and $\tau=150$ fs (case 4), $I=1.25\times10^{23}$ W/m^2 and $\tau=200$ fs (case 5), and $I=1\times10^{23}$ W/m^2 and $\tau=250$ fs (case 6). In the parameters we employed, a total energy of the laser injected is calculated by $E_{input}\sim\pi^{3/2}Ir_{spot}\tau/4=7.32\times10^4$ J/m, and if the laser is cylindrically symmetric, the total laser energy is estimated by $E_{input}\sim Ir_{spot}^2\tau\sim0.109$ J. In this paper, the target side illuminated by the laser is called the laser side and the other side is called the rear side. The calculation region is given by $R=\{(x,y)|0<x<50\lambda, 0<y<45\lambda\}$, and the foil is placed in $23.5\lambda\leqslant x\leqslant25\lambda$, and $10\lambda\leqslant y\leqslant35\lambda$ at the initial time of $t=0$. The mesh width in the x and y directions $\Delta=\Delta x=\Delta y=0.04\lambda$, the computational time step $\Delta t=0.0016\lambda/c$, and the total number of superparticles is equal to 3.75×10^5 for both electrons and protons, respectively. The laser center in the transverse direction is $y_c=22.5\lambda$. In the y direction, a periodic boundary is used, and a free boundary condition is employed in the x direction.

III. SIMULATION RESULTS

A. High-energy protons generated from the foil target

Figures 2 and 3 present numerical simulation results of the proton acceleration. Figure 2 shows developments of the total kinetic and fields energies for (a) case 1 and (b) case 6, and spectra of the proton kinetic energy at $t=660$ fs (case 1) and $t=990$ fs (case 6) are presented in Figs. 3(a) and 3(b), respectively. In these times, the electrons and protons have already reached the quasi steady state. In Fig. 3, the protons, whose longitudinal velocity is $v_x\geqslant0$, are called the forward protons and the others ($v_x<0$) called the backward protons. In our parameters of the foil and laser, the electrons mainly obtain a net energy from the ponderomotive force of the laser and the charge separation appears near both sides of the target surface. The protons are accelerated by the longitudinal electric field generated by the fast electrons. In the case of the intense short-pulse laser (case 1), the electron energy increases rapidly by the laser and its energies are transformed into electric and magnetic fields. Therefore the field energies increase around the time $t=150$ fs with the reduction of the electron energy as shown in Fig. 2(a). At this time, a strong electric field (a few MV/μm) exists near both sides of the target and a magnetic field (a few kT) is also produced. Such an electric field accelerates the protons. On the other hand, in case 6, the electrons are accelerated gradually because of the long-pulse and low-intensity laser. Therefore compared with that in case 1, a long time is required until the protons reach to the quasi steady state. After proton acceleration, the maximum kinetic energies of the forward and backward protons reach about 8 MeV and 4 MeV, respectively, for both cases 1 and 6 as shown in Figs. 3(a) and 3(b).

An energy conversion efficiency from the laser to the total protons for case 1 is $\eta_p=8.44\%$ and it is slightly smaller than

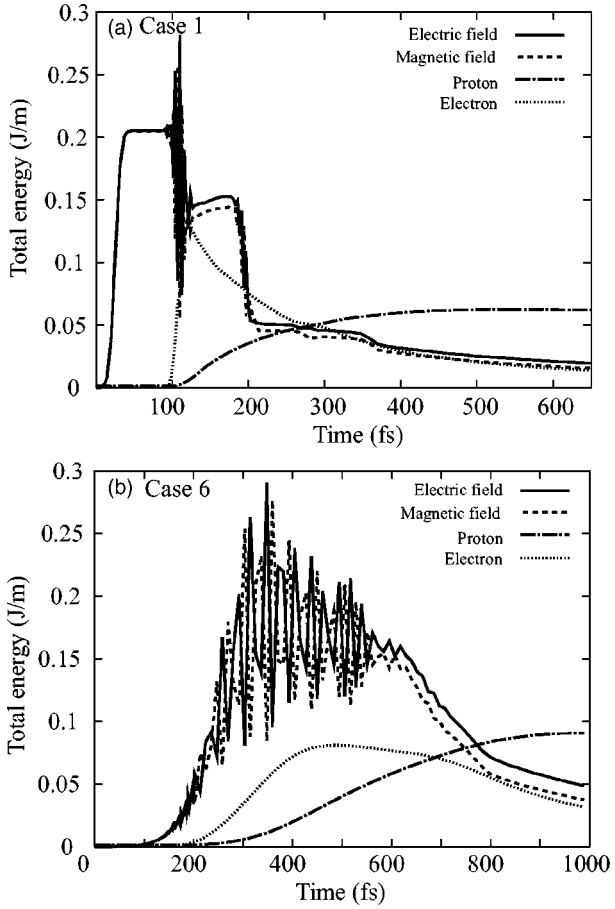

FIG. 2. Time developments of the total kinetic and fields energies in the computational region for the parameter sets of (a) case 1 and (b) case 6.

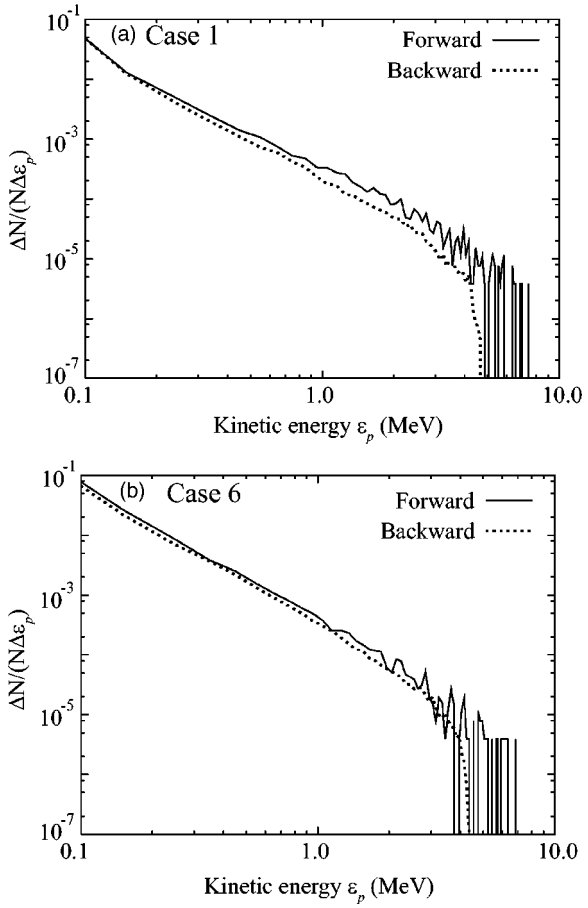

FIG. 3. Energy spectra of the proton kinetic energy ε_p in the cases of (a) case 1 and (b) case 6. Here "forward" means the protons of $v_x \geqslant 0$, "backward" indicates the protons of $v_x < 0$, and N is the total proton number.

that in the case of case 6 ($\eta_p = 12.4\%$). However, the energy conversion efficiency from the laser to the high-energy protons ($\geqslant 500$ keV) is almost the same for both case 1 ($\eta_p = 3.17\%$) and case 6 ($\eta_p = 3.55\%$). Although the target heating efficiency by the laser becomes high for the long-pulse laser, the energy transfer efficiency to the protons accelerated from the laser is not influenced strongly by the laser parameters, if the laser input energy is kept constant. Such a proton acceleration mechanism by charge separation was studied in previous research [16]. In the following subsection, the suppression mechanism of the transverse protons divergence is described in detail.

B. Localization of the electrons

As shown in the previous subsection, the protons are accelerated by the longitudinal electric field for both the intense short-pulse laser and the low-intensity and long-pulse laser, and the maximum kinetic energy of the proton reaches about 8 MeV. Although the proton maximum kinetic energy is not influenced much, when the laser input energy is fixed, the distributions of the electric and magnetic fields become different by changing the laser parameters. If the laser intensity is enough high ($a_0 \geqslant 1$), the laser accelerates the electron energy to the relativistic energy by the ponderomotive force. Here $a_0 = eE_0/(m_e \omega_L c)$ is the dimensionless parameter of the laser electric field, e is the electron charge, E_0 is the amplitude of the laser electric field, ω_L is the laser angular frequency, and c is the speed of light in vacuum. In the laser parameters employed, $a_0 > 1$. Figure 4 shows distributions of high-energy ($\varepsilon_e \geqslant 1$ MeV) electrons and the critical density surface in the x-y plane in the cases of (a) case 1 ($t = 112$ fs) and (b) case 6 ($t = 337$ fs), respectively. In these cases, the laser peak reaches the target at $t = 107$ fs (case 1) and $t = 332$ fs (case 6), respectively. From Fig. 4(a), because the laser intensity increases rapidly spatially, the strong ponderomotive force accelerates the electrons and the local fast electron bunches are generated clearly in the thin foil target. The laser propagates in the part of the underdense and is reflected by the foil around the critical density surface. Therefore the curvatures of the electron bunches almost agree with the critical density surface, and distances of the electron bunches correspond to a half of the laser wavelength $\lambda/2$. On the other hand, the electrons in case 6 are gradually accelerated and scattered in the transverse direction by the laser, and consequently high-energy electron bunches are not formed clearly in the foil target. Figure 5 presents the peak electron kinetic energy densities for all cases. From Fig. 5, the electron energy density increases with a reduction in the laser pulse duration.

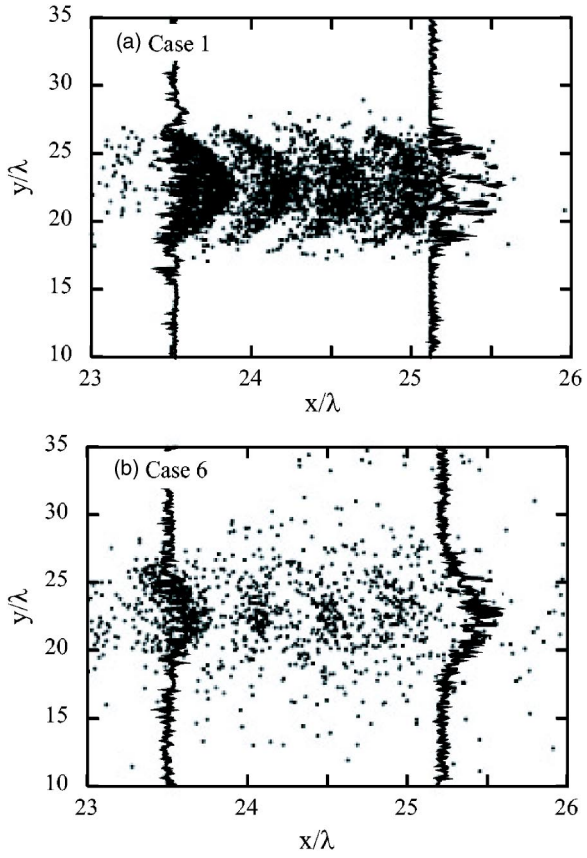

FIG. 4. Distributions of the high-energy ($\varepsilon_e \geqslant 1.0$ MeV) electrons and the critical density surface of $n_c = 1.01 \times 10^{27}$ m^{-3} for (a) case 1 and (b) case 6, respectively.

After the laser accelerates the electrons, the fast electron bunches run away from the target to the rear side domain and produce the electric and magnetic fields. The structures of such the fields change with the laser parameters. The fast electrons produce a high current, and thereby a strong magnetic field, which has a confinement effect for the electrons, is produced at the target surface. Figure 6 presents the time revolutions of the magnetic field B_z^{avg} distributions in the x-y plane for cases 1 and 6, respectively. Here the magnetic field B_z^{avg} is averaged by one laser period. In the case of the intense short-pulse laser (case 1), the fast electron bunches

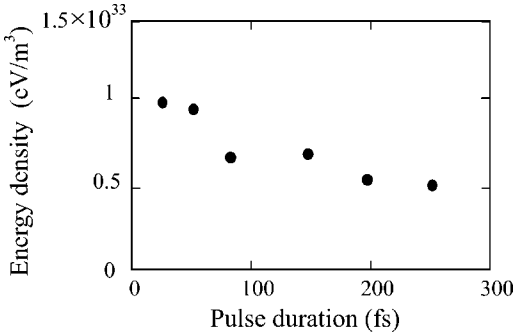

FIG. 5. The maximum energy densities of the electrons for all the cases. The energy density shows the maximum in the interaction with the laser for all the parameter sets.

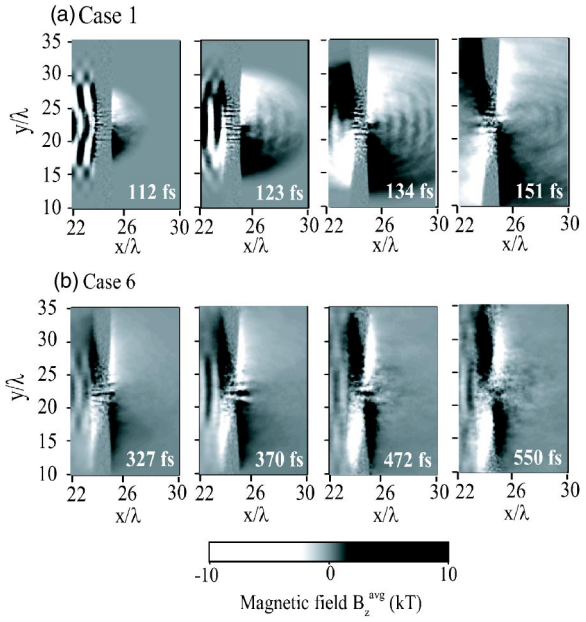

FIG. 6. Time developments of the magnetic field B_z^{avg} in the x-y plane for (a) case 1 and (b) case 6, respectively. Here the magnetic field is averaged by one laser period. The peak of the laser intensity reaches to the left end of the foil target at the time of (a) $t = 107$ fs and (b) $t = 332$ fs, respectively.

produce a strong magnetic field B_z^{avg} of the order of 1 kT at both target surfaces. Even in the case of the low-intensity and long-pulse laser (case 6), the magnitude of the magnetic field B_z^{avg} reaches the order of 1 kT at the target surfaces. However, the region of the strong magnetic field is thin [see Fig. 6(b)] compared with that in case 1 [see Fig. 6(a)]. The maximum magnitudes of the magnetic field $|B_z^{avg}|_{max}$ in cases 1 and 6 reach 8.17 kT (123 fs) and 5.31 kT (337 fs), respectively, and the widths of the strong magnetic field domain ($\geqslant |B_z^{avg}|_{max}/10$) from the right side of the target are 3.68λ (case 1) and 2.56λ (case 6), respectively. The distributions of the charge density in the x-y plane for cases 1 and 6 are presented in Fig. 7. The solid lines indicate an area of negative charge density of ($\leqslant \rho_0^{min}/5$), where ρ_0^{min} is the minimum charge density for each case. In case 1, the ponderomotive force compresses and accelerates the electrons longitudinally. Moreover, the electrons accelerated are confined by the magnetic field in transverse, and consequently a high-density electron bunch is produced and localized in the narrow domain at the rear side region. On the other hand in case 6, because the electrons accelerated gradually by the long-pulse laser are not compressed enough in the longitudinal direction and are scattered in transverse, the size of the electron bunch becomes large and the density decreases. The minimum charge density at the rear side is $\rho_0^{min} = -4.90 \times 10^7$ C/m^3 (case 1) and $\rho_0^{min} = -2.02 \times 10^7$ C/m^3 (case 6).

The localization of the negative charge is related to the magnitude of the magnetic field and the expansion of the electron caused by the space charge effect. An analytical estimation of the localization of the negative charge in transverse is presented below. In order to estimate the suppression effect for the electrons, we assume that the electron bunch

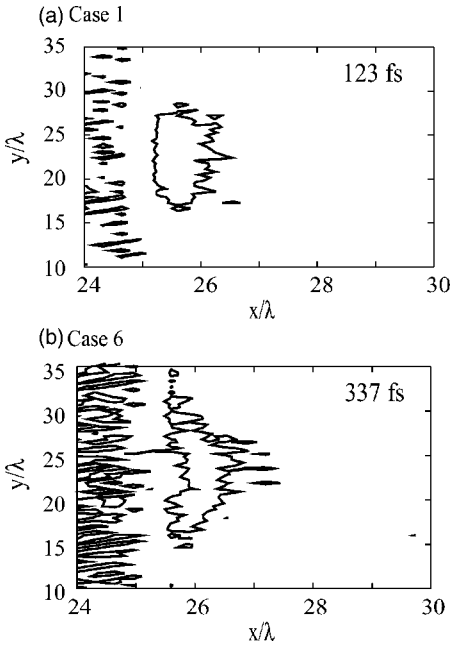

FIG. 7. Distributions of the charge density in the *x*-*y* plane at $t=123$ fs (case 1) and $t=337$ fs (case 6). Here the solid lines show a negative charge density of $\rho_0^{min}/5$ for cases 1 and 6, where ρ_0^{min} means the minimum charge density. For case 1, $\rho_0^{min}=-4.90\times10^7$ C/m^3, and for case 6, $\rho_0^{min}=-2.02\times10^7$ C/m^3.

forms an ellipsoid in the $x-y$ plane with a uniform density. Figure 8 shows a calculation model for estimation of the transverse electron confinement. The center of the ellipsoid electron bunch (x_0,y_0) is assumed by the averaged values of the electron positions, which exist inside the area of negative charge density of $\rho_0^{min}/5$. The semiaxis of the ellipsoid electron bunch is estimated by the rms value of the difference in position from the beam center: $\tilde{a}=[\overline{(x-x_0)^2}]^{1/2}$ and $\tilde{b}=[\overline{(y-y_0)^2}]^{1/2}$, respectively. The space charge potential inside the ellipsoid electron bunch with a uniform charge density is written by [24,25]

$$\phi_i = -\frac{\rho_0}{2\varepsilon_0}\frac{\tilde{b}x^2+\tilde{a}y^2}{\tilde{a}+\tilde{b}}, \tag{1}$$

where ϕ_i is the space charge potential inside the beam and ε_0 is the permittivity in vacuum. From the above equation, a

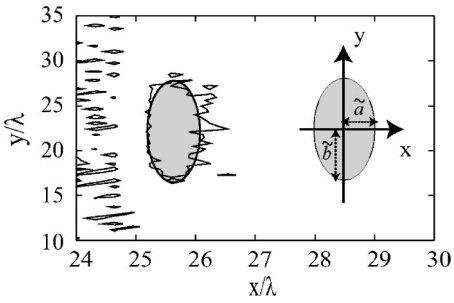

FIG. 8. Schematic view of the estimation model of the electron confinement effect. Here $\tilde{a}$ and $\tilde{b}$ present the semiaxes of the ellipsoid electron bunch in the *x* and *y* directions.

transverse force of the electric field produced by the space charge effect can be estimated by

$$F_y^{ele} < F_y^{mag} = -e\frac{\partial\phi_i}{\partial y} = -e\frac{\rho_0}{\varepsilon_0}\frac{\tilde{a}y}{\tilde{a}+\tilde{b}}. \tag{2}$$

From the Maxwell equations, the magnetic field B_z and its force F_y^{mag} are given by

$$B_z = \mu_0\rho_0 c\beta_e y, \tag{3}$$

$$F_y^{mag} = e\frac{\rho_0}{\varepsilon_0}\beta_e^2 y. \tag{4}$$

Here μ_0 is the permeability, β_e is the averaged velocity of the ellipsoid electron bunch normalized by *c*, and the transverse component of the current is assumed to be zero. If $F_y^{ele} < F_y^{mag}$, the electrons are confined by the magnetic field. Finally the condition for the confinement of the electrons can be expressed by

$$\beta_e > \sqrt{\tilde{a}/(\tilde{a}+\tilde{b})}. \tag{5}$$

In case 1, the center of the ellipsoid electron bunch $(x_0,y_0)=(25.7\lambda,22.4\lambda)$, the electron velocity in the *x* direction is $\beta_e=0.350$, and the semiaxes of the ellipsoid bunch in the *x* and *y* directions are $\tilde{a}=0.206\lambda$ and $\tilde{b}=2.04\lambda$, respectively. Therefore $\sqrt{\tilde{b}/(\tilde{a}+\tilde{b})}=0.303$, and consequently the suppression condition expressed in Eq. (5) is satisfied. At case 6, the center of the ellipsoid electron bunch $(x_0,y_0)=(25.9\lambda,23.1\lambda)$, the electron velocity in the *x* direction is $\beta_e=0.200$, the semiaxes of the ellipsoid bunch in the *x* and *y* directions are $\tilde{a}=0.425\lambda$ and $\tilde{b}=3.89\lambda$, and then $\sqrt{\tilde{b}/(\tilde{a}+\tilde{b})}=0.314$. The suppression condition is not satisfied in this case. Consequently the electrons expand in the transverse direction by the space charge effect in case 6. Figure 9(a) shows the relations between the bunch size $\tilde{a}$ and the beam velocity β_e normalized by *c*. The transverse bunch size $\tilde{b}$ is assumed to be 3.00λ. In Fig. 9, the suppression condition is satisfied in the area above the solid line. From Fig. 9(a), the suppression condition is influenced strongly by the longitudinal bunch size of $\tilde{a}$. If $\tilde{a}\gg\tilde{b}$, because the space charge effect strongly appears in the transverse direction, the electron velocity has to be close to the speed of light *c* [see Eq. (5)]. Figure 9(b) presents the simulation results and its thresholds. The circles and triangles show the simulation result and threshold for all cases, respectively. In cases 1 and 2, the suppression condition is satisfied well. In case 2, the semiaxes of the electron bunch in the *x* and *y* directions are $\tilde{a}=0.180\lambda$, and $\tilde{b}=2.46\lambda$, respectively. Because the magnetic field confines the electrons in case 1, the transverse size of the ellipsoid electron bunch ($\tilde{b}=2.04\lambda$) becomes small, and the electrons are slightly expanded in the longitudinal ($\tilde{a}=0.206\lambda$) direction. Therefore the longitudinal size of the ellipsoid electron bunch is larger than that in case 2. With an increase of the pulse length and reduction of the laser intensity, the electron bunch size becomes large in the transverse and longitudinal directions and its velocity decreases as

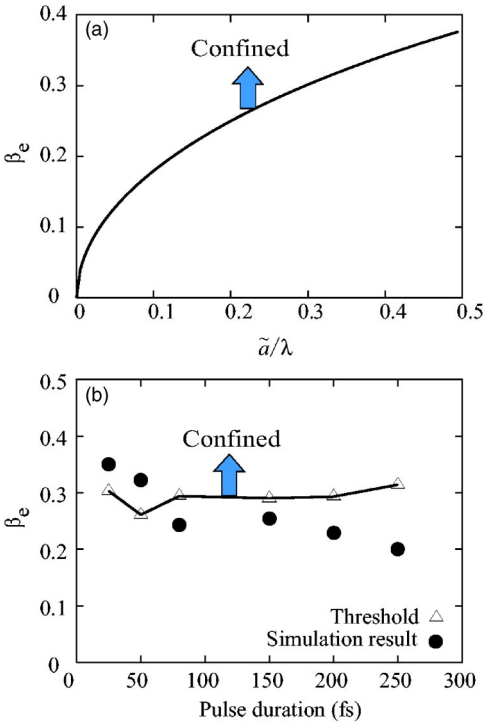

FIG. 9. (a) Relation of the longitudinal electron bunch size $\tilde{a}$ and the electron velocity β_e to satisfy the suppression condition of the electrons. Here the electron bunch velocity is normalized by c, and the suppression condition is satisfied in the domain above the solid line. (b) Simulation results (the circle) and its threshold (the triangle) for all the cases.

shown in Fig. 9(b). Consequently the electron bunch can not satisfy the suppression condition in cases 3–6.

C. Suppression of the proton divergence in the transverse direction

Time developments of the transverse and longitudinal electric fields in the x-y plane for case 1 and case 6 are shown in Figs. 10 and 11, respectively. Here the electric fields are averaged over the one laser period. The intense short pulse laser (case 1) compresses the electrons longitudinally and the magnetic field confines the electrons in the transverse direction at the rear side region. Consequently the longitudinal electric field is formed strongly and a transverse electric field toward the laser axis appears. At this time, most protons are not yet emitted from the foil target because of the difference of the mass ratio between the electron and proton. For case 1, the maximum magnitudes of the transverse and longitudinal electric fields reach 11.0 MV/μm and 3.73 MV/μm, respectively. The protons are accelerated strongly by the longitudinal electric field and at the same time the protons emitted are extracted to the central axis by the transverse electric field in the rear side region. After the protons are emitted in the rear side region, the effect of the electrons localization influences greatly the suppression of the transverse dispersion of the proton, although the local negative charge is neutralized by the protons charge and consequently the transverse electric field, which has the suppression effect for the protons vanishes. From Fig. 10(b), in the case of the low-intensity and long-pulse laser (case 6), the electrons are not compressed longitudinally, and the maximum magnitude of the longitudinal electric field is 64.7% of that in case 1, although the peak of the longitudinal electric

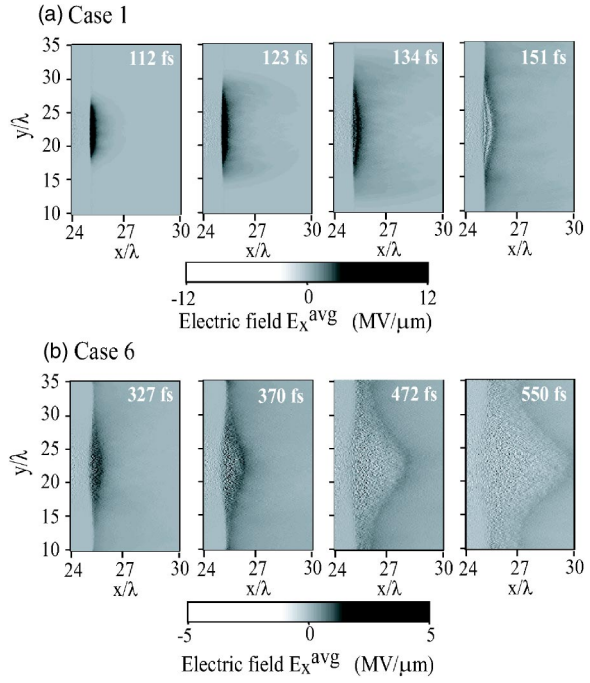

FIG. 10. Time developments of the longitudinal electric field E_x^{avg} in the x-y plane at the times of the foil interacted strongly with the laser pulse for (a) case 1 and (b) case 6, respectively. The electric fields are normalized by the laser period.

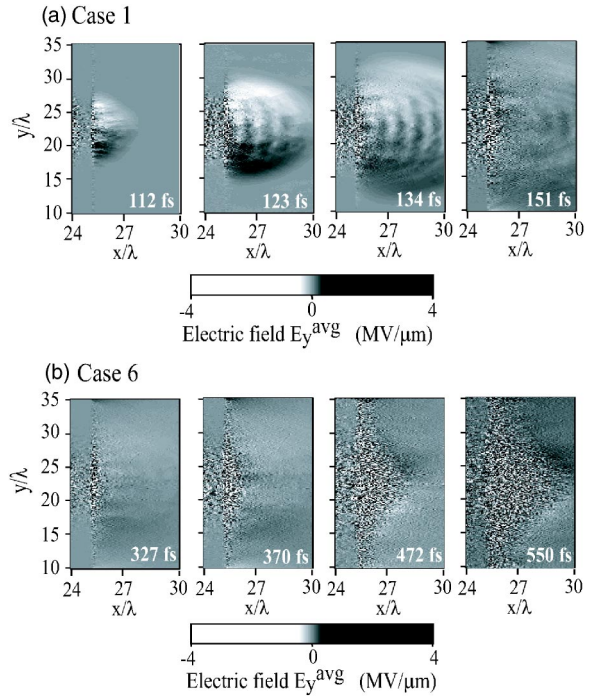

FIG. 11. Time developments of the transverse electric field E_x^{avg} in the x-y plane for (a) case 1 and (b) case 6.

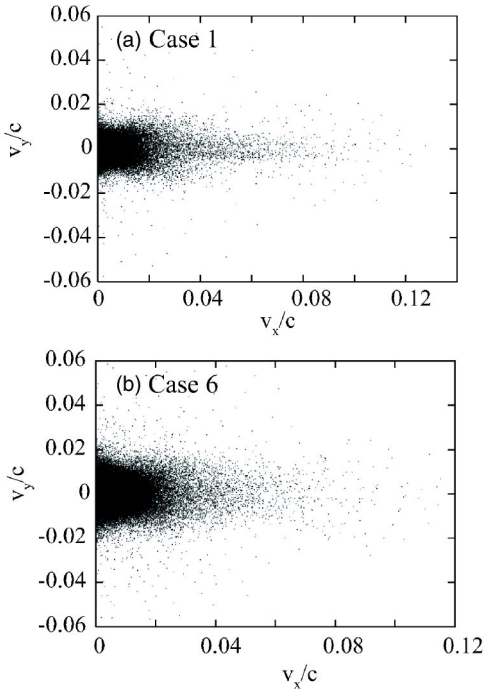

FIG. 12. Phase space v_x-v_y distributions at time of $t=750$ fs (case 1) and $t=990$ fs (case 6), respectively. Here the velocity is normalized by c. For each case, the proton and electron energies have reached the quasi steady state.

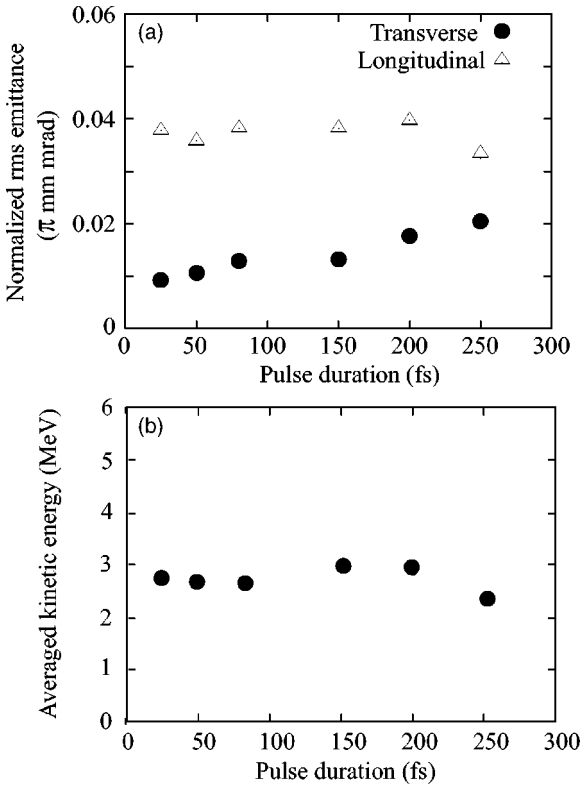

FIG. 13. (a) Normalized transverse and longitudinal rms emittances and (b) the averaged kinetic energies of the protons accelerated for all cases.

field is weak and the laser interacts with the foil and provides electrons for a long time. Therefore the protons are accelerated and emitted gradually. The localization of the electrons does not appear because the magnitude of the magnetic field is weak and the region of the strong magnetic field is also narrow as shown in Fig. 6. Therefore the transverse electric field, which attracts the protons to the central axis, is not produced clearly as shown in Fig. 11(b).

Figure 12 shows phase space v_x-v_y distributions of the forward protons ($v_x>0$) for (a) case 1 and (b) case 6, respectively. In each case, the protons have reached the quasi steady state. The protons are accelerated strongly in the longitudinal direction in all cases, and moreover for intense short-pulse laser, the local electron bunch extracts the protons to the central axis as described above. Consequently the transverse expansion of the protons accelerated is smaller than that in the low-intensity and long-pulse laser. Figure 13 presents (a) normalized longitudinal and transverse rms emittances of the proton bunch accelerated and (b) the averaged kinetic energy of proton bunch accelerated for all the cases. The normalized longitudinal and transverse rms emittances are expressed by [24]

$$\varepsilon_x = \gamma_0\beta_0[\overline{(x-x_0)^2}]^{1/2}\frac{[\overline{(P_x-P_0)^2}]^{1/2}}{P_0}, \tag{6}$$

$$\varepsilon_y = \gamma_0\beta_0[\overline{(y-y_0)^2(y'-y'_0)^2}-\overline{(y-y_0)(y'-y'_0)^2}]^{1/2}. \tag{7}$$

Here γ_0 is the averaged relativistic factor of the beam, β_0 is the averaged beam velocity normalized by c, x_0 and y_0 are the center of the beam, $y'=P_y/P_0$ is the rms divergence, P_x and P_y are the particle momentum in the x and y directions, and P is the averaged beam momentum. The influences of the laser parameters on the longitudinal proton divergence and the averaged kinetic energy protons accelerated are weak. For all cases, the longitudinal rms emittance is about $(0.03-0.04)\pi$ mm mrad, and the averaged kinetic energy of the proton bunch accelerated reaches about 3 MeV. However, the transverse rms emittance increases with a reduction of the laser intensity and with an increase of the laser pulse duration. The transverse rms emittance of case 1 is $(0.920\times10^{-2})\pi$ mm mrad, and it is 40.2% of that in case 6. In Figs. 12 and 13, one can see the suppression effect of the transverse proton divergence by using the intense short-pulse laser.

In the previous subsection, we discussed about the electron confinement effect by the magnetic field, which is generated by the electrons itself. Therefore the protons diverge in the transverse direction by such a magnetic field because the proton charge is positive. In order to investigate the divergence effect of the magnetic field to the protons, we calculated another case as shown below. Although the relativistic equation of motion is completely solved in the calculation, the magnetic field effect on the protons is omitted here—i.e., $d\mathbf{P}/dt=q\mathbf{E}$ (only for the protons). Here $\mathbf{P}$ is the momentum of the proton. From the calculation results, the transverse rms emittance for case 1 is 0.892π mm mrad, and the difference between these two cases is about 3.14%. The difference of the averaged kinetic energy between both

the calculation conditions is 2.17%. From the above simulation results, one can find that the magnetic field does not contribute much to the transverse divergence of the protons.

IV. CONCLUSIONS

In this paper, we proposed a suppression mechanism of the transverse proton divergence. In our 2.5-dimensional PIC simulation, the lasers of six different cases of laser intensity and pulse duration illuminate the hydrogen thin foil target. The laser input energy is kept constant in all cases. The simulation results show that the electrons are strongly accelerated and compressed by the ponderomotive force in the laser direction and charge separation is caused rapidly at both the sides of the foil target in the case of the intense (1.0×10^{24} W/m^2) short-pulse (25 fs) laser. At this time, the electrons are confined by the strong magnetic field generated by the fast electrons itself at the opposite side of the laser irradiated. The electrons confined produce the local electron bunch in the transverse and longitudinal directions at the rear side domain. The maximum amplitude of the magnetic field reaches 8.17 kT. Although the magnetic field reaches a few kT in the case of a low-intensity (1.0×10^{23} W/m^2) and long-pulse (250 fs) laser, the magnitude of the magnetic field is 5.31 kT, and it is 65.0% of that in the intense short-pulse laser. Consequently the magnetic field does not confine well the electrons in the transverse direction and localization of the electrons cannot be observed clearly.

In our study, estimation of the electron confinement effect is also performed in Sec. II. From the estimation results, one of the important parameters of the confinement mechanism for the electrons is the longitudinal electron bunch size. The electron bunch requires high speed and small size in the longitudinal direction to satisfy the suppression condition of the proton beam transverse divergence.

The comparisons among the proton beam qualities for all cases are shown in Sec. II. From the calculation results, the transverse proton divergence mainly comes from the electric field, not from the magnetic field, and the transverse rms emittance of the protons accelerated increases with the reduction of the laser intensity. The proton energy is almost same for all cases on the fixed laser input energy. In all cases, the average kinetic energy of the protons accelerated reaches about 3 MeV, and the longitudinal rms emittance is $(0.03-0.04)\pi$ mm mrad. However, the transverse rms emittance of the protons accelerated has a remarkable difference for the laser parameters. At the laser intensity of 1.0×10^{24} W/m^2 and pulse duration of 25 fs (case 1), the transverse rms emittance is $(0.920\times10^{-2})\pi$ mm mrad, and it is 45.2% of that in the case of an intensity of 1.0×10^{23} W/m^2 and pulse duration of 250 fs (case 6).

ACKNOWLEDGMENTS

This work is partly supported by the JSPS (Japan Society for the Promotion of Science) and MEXT (Ministry of Education, Culture, Sports, Science and Technology). We would like present our thanks to Professor K. Mima, Professor K. Tachibana, Professor A. A. Andreev, Professor S. V. Bulanov, Professor J. Limpouch, Professor K. Nakajima, Professor S. Kurokawa, Dr. K. Nemoto, and Professor N. Yugami for their valuable discussions and suggestions on this subject.

[1] D. Strickland and G. Mourou, Opt. Commun. **56**, 219 (1985).
[2] G. Mourou, C. P. J. Barty, and M. D. Perry, Phys. Today **51**(1), 22 (1998).
[3] G. Malka, E. Lefebvre, and J. L. Miquel, Phys. Rev. Lett. **78**, 3314 (1997).
[4] B. Hafizi, A. Ting, E. Esarey, P. Sprangle, and J. Krall, Phys. Rev. E **55**, 5924 (1997).
[5] G. V. Stupakov and M. S. Zolotorev, Phys. Rev. Lett. **86**, 5274 (2001).
[6] S. Miyazaki, Q. Kong, S. Kawata, and J. Limpouch, J. Phys. D **36**, 2878 (2003).
[7] Q. Kong, S. Miyazaki, S. Kawata, K. Miyauchi, K. Sakai, Y. K. Ho, K. Nakajima, N. Miyanaga, J. Limpouch, and A. A. Andreev, Phys. Rev. E **69**, 056502 (2004).
[8] K. Miyauchi, S. Miyazaki, K. Sakai, and S. Kawata, Phys. Plasmas **11**, 4878 (2004).
[9] S. C. Wilks, Phys. Fluids B **5**, 2603 (1993).
[10] T. Nakamura and S. Kawata, Phys. Rev. E **67**, 026403 (2003).
[11] K. Matsukado *et al.*, Phys. Rev. Lett. **91**, 215001 (2004).
[12] T. E. Cowan *et al.*, Phys. Rev. Lett. **92**, 204801 (2004).
[13] A. A. Andreev, K. Yu. Platonov, T. Okada, and S. Toraya, Phys. Plasmas **10**, 220 (2003).
[14] J. Denavit, Phys. Rev. Lett. **69**, 3052 (1992).
[15] E. L. Clark, K. Krushelnick, M. Zepf, F. N. Beg, M. Tatarakis, A. Machacek, M. I. K. Santala, I. Watts, P. A. Norreys, and A. E. Dangor, Phys. Rev. Lett. **85**, 1654 (2000).
[16] K. Nemoto, A. Maksimchuk, S. Banerjee, K. Flippo, G. Mourou, D. Umstadter, and V. Yu. Bychenkov, Appl. Phys. Lett. **78**, 595 (2001).
[17] S. V. Bulanov, T. Zh. Esirkepov, V. S. Khoroshkov, A. V. Kuznetsov, and F. Pegoraro, Phys. Lett. A **299**, 240 (2002).
[18] M. Allen *et al.*, Phys. Plasmas **10**, 3283 (2003).
[19] S. V. Bulanov, T. Zh. Esirkepov, J. Koga, T. Tajima, and D. Farina, Plasma Phys. Rep. **30**, 21 (2004).
[20] M. Borghesi, A. J. Mackinnon, D. H. Campbell, D. G. Hicks, S. Kar, P. K. Patel, D. Price, L. Romagnani, A. Schiavi, and O. Willi, Phys. Rev. Lett. **92**, 055003 (2004).
[21] T. Esirkepov, M. Borghesi, S. V. Bulanov, G. Mourou, and T. Tajima, Phys. Rev. Lett. **92**, 175003 (2004).
[22] S. C. Wilks, A. B. Langdon, T. E. Cowan, M. Roth, M. Singh, S. Hatchett, M. H. Key, D. Pennington, A. MacKinnon, and R. A. Snavely, Phys. Plasmas **8**, 542 (2004).
[23] M. Hegelich *et al.*, Phys. Rev. Lett. **89**, 085002 (2002).
[24] M. Reiser, *Theory and Design of Charged Particle Beams* (Wiley, New York, 1994).
[25] I. Hofmann and J. Struckmeier, Part. Accel. **21**, 69 (1987).